Materials Science Forum Vol. 767 (2014) pp 13-21
Online available since 2013/Jul/31 at www.scientific.net

doi:10.4028/www.scientific.net/MSF.767.13

Computational Analysis of Ignition in Heterogeneous Energetic Materials

Ananda Barua[1,a], Seokpum Kim[1,b], Yuki Horie[2] and Min Zhou[1,d]

[1]The George W. Woodruff School of Mechanical Engineering, School of Materials Science and Engineering. Georgia Institute of Technology, Atlanta, Georgia 30332-0405, USA

[2]Air Force Research Lab, Munitions Directorate, 2306 Perimeter Road, Eglin AFB, FL 32542, USA

[a]abarua@gatech.edu, [b]seokpumkim@gatech.edu, [c]yasuyuki.horie@eglin.af.mil, [d]min.zhou@gatech.edu

Keywords: PBX, energetic materials, ignition, dynamic response, modeling

Abstract. This paper focuses on the ignition of polymer-bonded explosives (PBXs) under conditions of non-shock loading. The analysis uses a recently developed ignition criterion [1] which is based on the quantification of the distributions of the sizes and temperatures of hotspots in loading events. This quantification is achieved by using a cohesive finite element method (CFEM) developed recently and the characterization by Tarver et al. [2] of the critical size-temperature threshold of hotspots required for chemical ignition of solid explosives. Calculations are performed on PBXs having monomodal grain size distributions with grain volume fractions varying between 0.72 and 0.90. The impact velocities considered vary between 100 and 200 ms^{-1}. Results show that the average distance between the hotspots is dependent on the grain volume fraction. As the grain volume fraction increases, the time to criticality (t_c) decreases, signifying increases in the ignition sensitivity of PBX to impact loading. The microstructure-performance relations obtained can be used to design PBXs with tailored performance characteristics and safety envelopes.

Introduction

The issue of impact-induced ignition in energetic materials has received significant attention over the past few decades [3-6]. Ignition can occur as a result of energy localization in the form of local temperature increases or hotspots. A number of thermomechanical processes occur simultaneously subsequent to impact loading and it is not straightforward to ascribe the ignition to one particular cause [7]. Impact-induced-initiation can be roughly divided into two regimes of interest: shock and non-shock conditions. A comprehensive survey of the shock response of energetic materials can be found in [8]. Here, we focus on non-shock conditions.

Several researchers have focused on computational modeling of impact-induced initiation. Relevant works include the modeling of heterogeneous microstructures at the mesoscale (Baer [3, 9-10], Benson et al. [11-12]), shock response of porous explosives (Hayes [13]), compaction of granular HMX (Menikoff [14-15]), chemical reaction and hotspot formation (Dlott [16-17]), micromechanical burn of solid explosives (Hamate and Horie [6]), and chemical kinetics of reaction in pure explosives (Tarver et al. [2], Henson et al. [8]), among others. Gonthier et al. [18] performed mesoscale simulations of impact loading of granular explosives. Barua et al. [19-21] developed a novel capability based on the cohesive finite element method (CFEM) for analyzing the thermal and mechanical responses of heterogeneous energetic materials. Dienes et al. [22] studied the impact initiation of explosives using statistical crack mechanics. This approach accounts for crack growth and coalescence. Frictional heating caused by sliding of crack faces can also be analyzed. The authors showed that the overall load-displacement response using the approach matches well with experimental results. However, since microstructure is not considered, the spatial distribution of quantities is not captured explicitly.

Recently, Barua et al. [1] developed an ignition criterion based on the conditions of mechanical loading and microstructural attributes. This was accomplished by considering the two phenomena, hotspot generation and local temperature evolution under influence of chemical reactions, as separate

but related processes. The former is concerned with the quantification of the contributions of different dissipation/heating mechanisms and how the contributions evolve as deformation progresses. This task is achieved through use of a recently developed Lagrangian cohesive finite element framework to quantify the effects of microstructure and thermal-mechanical processes such as matrix deformation, interfacial debonding and fracture of grains on hotspot formation. The latter (thermo-chemical runaway) is solved independently of hotspot dynamics – they are in essence "borrowed" from the existing work. The critical hotspot-size combinations form the threshold that taken as a material attribute. Such threshold relations are obtained using chemical kinetics calculations [2, 8].

The objective of this work is to use the ignition criterion developed by Barua et al. [1] to analyze the ignition sensitivity of PBXs having a range of grain volume fractions. This analysis is carried out over a range of impact velocities to develop an ignition threshold in terms of the impact velocity and the critical time (t_c) to ignition. Additionally, the spatial distributions of hotspots and their sizes are characterized by using a temperature threshold and calculating the radial distribution function (RDF) of the resultant hotspot field [1]. The analysis will help create microstructure-performance maps for the development of PBXs with tailored attributes.

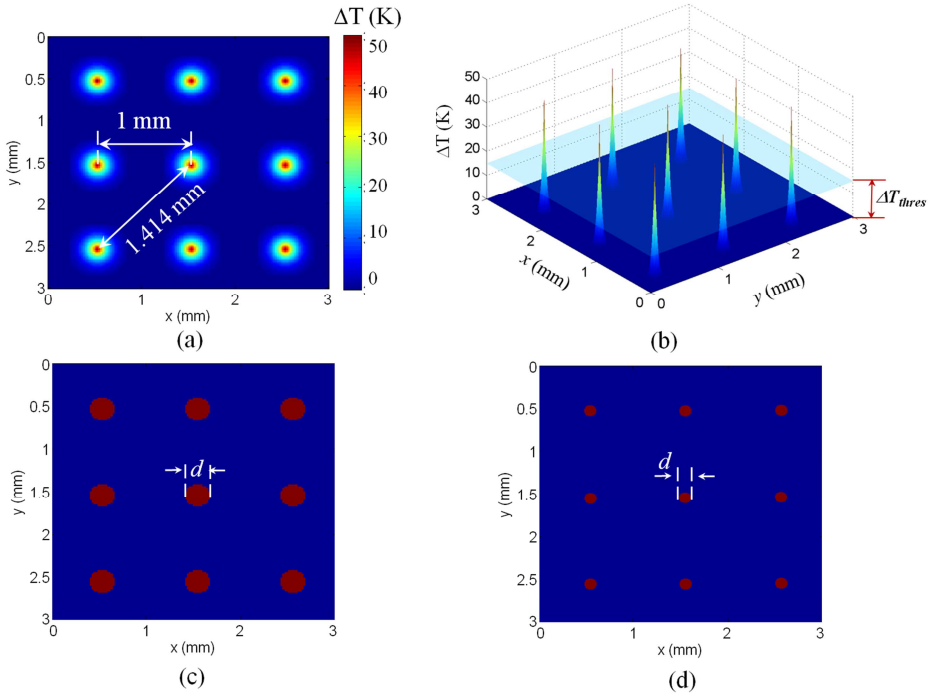

Fig. 1 Illustration and quantification of an idealized hotspot field, (a) hotspots arranged in a regular square array, (b) 3D temperature profile of the idealized hotspots field, and a schematic sectioning of the hotspot field by a plane at a given cutoff temperature, ΔT_{thres}., (c) hotspots on section with $\Delta T_{thres} = 15$ K, and (d) hotspots on section with $\Delta T_{thres} = 30$ K.

Ignition Criterion

The ignition criterion establishes the ignition conditions of heterogeneous energetic materials under general conditions (both shock and non-shock). This criterion links the hotspot size-temperature states in a loading event to the threshold size-temperature conditions of hotspots [2] which are regarded as materials properties. The ignition criterion is given in detail in [1] and only a brief description shall be provided here.

Mathematically, this criterion provides a relationship between the size and temperature of critical hotspots as,

$$d(T) \geq d_c(T), \tag{1}$$

where, d is the diameter of the dominant hotspot resulting from a loading event whose interior temperatures are at or above temperature T and d_c is the minimal diameter of a hotspot required for thermal runaway at temperature T.

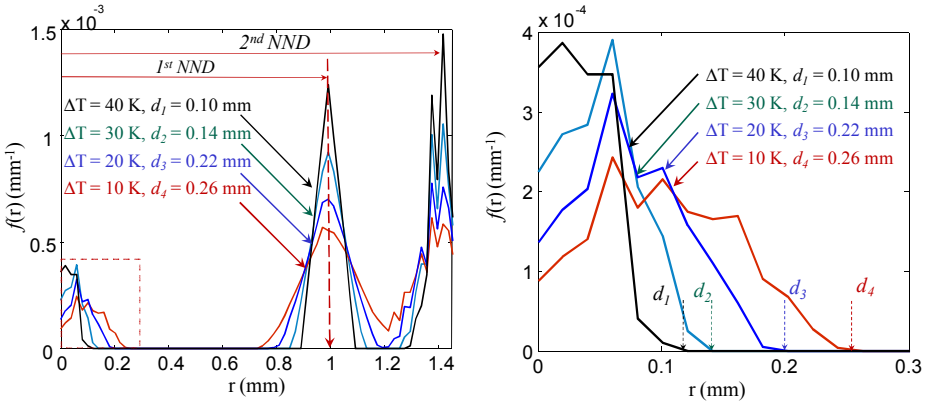

Fig. 2 (a) Radial distribution function (RDF) of the idealized hotspot field in Fig. 1 at different cutoff temperatures, and (b) a close-up view of the region where the RDFs go to zero which shows the diameter of the hotspots at the corresponding cutoff temperatures.

Statistical Characterization of Hotspot Field using Radial Distribution Function (RDF)

The size and temperature of hotspots need to be quantified prior to the application of any threshold criteria for ignition. To avoid the use of arbitrary size-temperature criteria in identifying hotspots, a novel scheme developed in [1] is used. This approach involves the use of a temperature threshold (ΔT_{thres}) which is of vital importance. At each time step, the microstructure is scanned for temperature rises above ΔT_{thres}. Areas of a temperature field with temperatures above the threshold are analyzed for hotspots. Successively varying ΔT_{thres} values allows the characteristics of a temperature field to be fully analyzed. In particular, strategically chosen threshold temperature values allow hotspots of interest to be identified.

To illustrate how this scheme works, Fig. 1(a) shows an idealized regular array of circular hotspots, each having a temperature rise of 50 K at the center and 0 K at the periphery. The variation of temperature inside the hotspots follows a smooth polynomial function. Figure 1(b) shows a 3D visualization of the temperature field with temperature as the vertical axis. A plane representing a threshold temperature of $\Delta T_{thres} = 15\,\mathrm{K}$ is shown intersecting the hotspot fields. Obviously, varying this ΔT_{thres} would reveal the hotspots and allow them to be quantified in different ways. These quantifications can be further analyzed to obtain more detailed statistical information.

The RDF describes how the density of a system of particles varies as a function of interparticle distance. Specifically, the RDF $f(r)$ represents the probability of finding a particle in a shell with thickness dr at a distance r from a particle. The radial distribution function profiles computed for the idealized hotspot distribution in Fig. 1 for $\Delta T_{thres} = 10, 20, 30$ and $40\,\mathrm{K}$ are shown in Fig. 2. At $r = 0, f(r)$ has a finite value. As r increases, $f(r)$ increases and decreases. The value of r at which $f(r)$ first

becomes zero corresponds to the maximum size of hotspots for a given ΔT_{thres} [see Fig. 2(b)]. As r further increases, two more peaks are observed, the first at $r = 1$ mm and second at 1.41 mm. These peaks correspond to the average nearest neighbor distance (NND) between the hotspots and the average second nearest neighbor distance, respectively. Note that the peaks become higher as the hotspot size decreases due to the normalization of the curves. Systematic characterizations of hotspots are presented in subsequent sections.

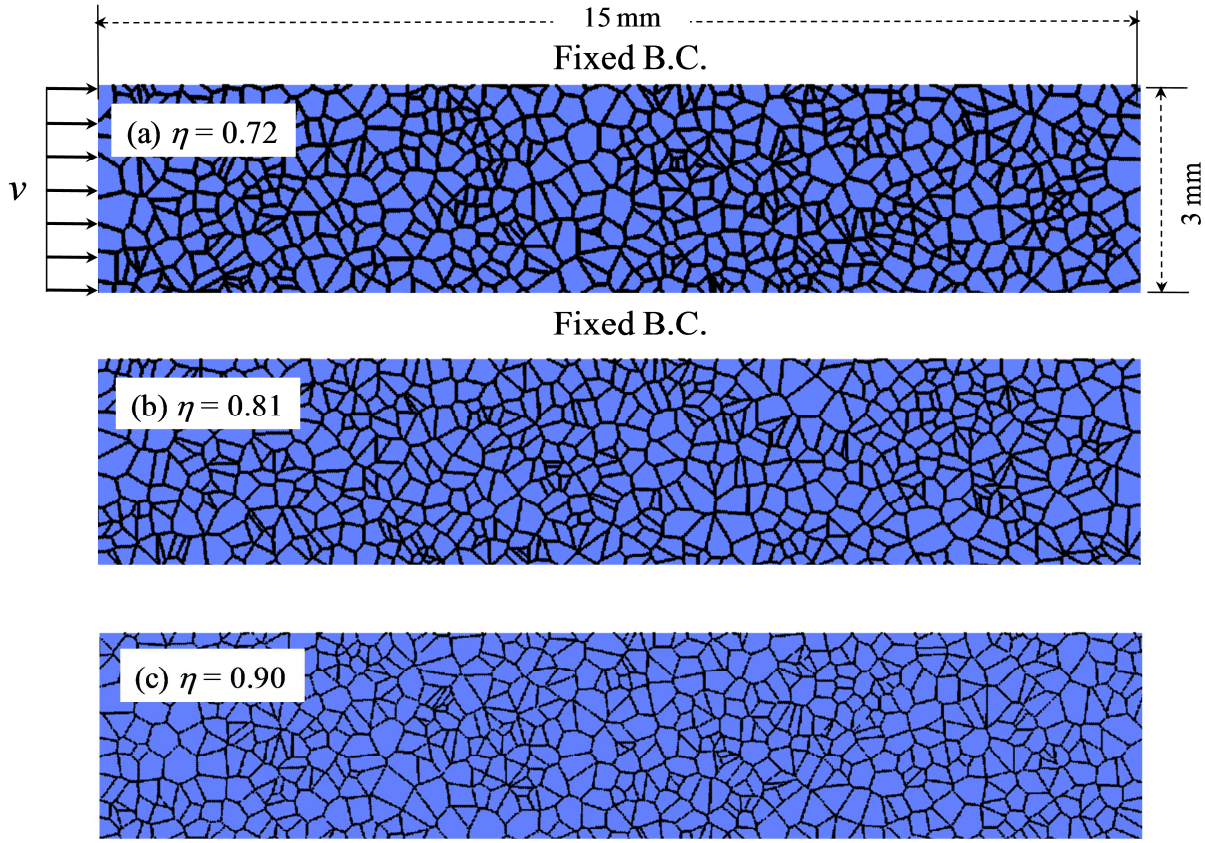

Fig. 3 (a) Loading configurations analyzed, the long specimens have an aspect ratio of 5:1 (15 mm × 3 mm); (a-c) Microstructures having a range of grain volume fractions ($\eta = 0.72 - 0.90$).

Microstructure Level Model

We focus on PBXs which have two-phase microstructures consisting of HMX grains and an Estane binder. Idealized microstructures are used to obtain samples with systematically varying attributes. A set of three idealized microstructures having monomodal size distribution are used to model the PBX. They are generated using Voronoi tessellation function in MATLAB. The packing density is varied by suitably altering the average thickness of the binder in between neighboring grains. The mean grain size is 250 μm with a standard deviation of 90 μm.

The loading configuration involves a $15\ \text{mm} \times 3\ \text{mm}$ rectangular microstructural region. This configuration is shown in Fig. 3(a). The upper and lower boundaries are constrained such that lateral expansion (up for the upper edge and down for the lower edge) does not occur. This configuration approximates the normal impact loading of an infinitely wide material block under conditions of macroscopic uniaxial strain. The imposed constant boundary/piston velocity approximately simulates loading under a constant input stress level. The specimen length is chosen to allow approximately the first 5.5-8.5 microseconds of the propagation of the stress wave from the left surface toward the right to be analyzed, before the wave arrives at the right end.

The calculations are carried out using the micromechanical cohesive finite element method (CFEM) framework developed by Barua et al. [19].

Results and Discussions

The calculations focus on the effects of (i) boundary velocity and (ii) grain volume fraction $(\eta = 0.72 - 0.90)$. For all calculations presented, the initial temperature is $T_i = 300\,\text{K}$. The imposed boundary velocity v is varied between 100 and 200 ms^{-1}. Since the configuration in Fig. 3(a) focuses on the transient response of microstructures, the relevant discussions are limited to times before the stress wave reaches the boundary on the right.

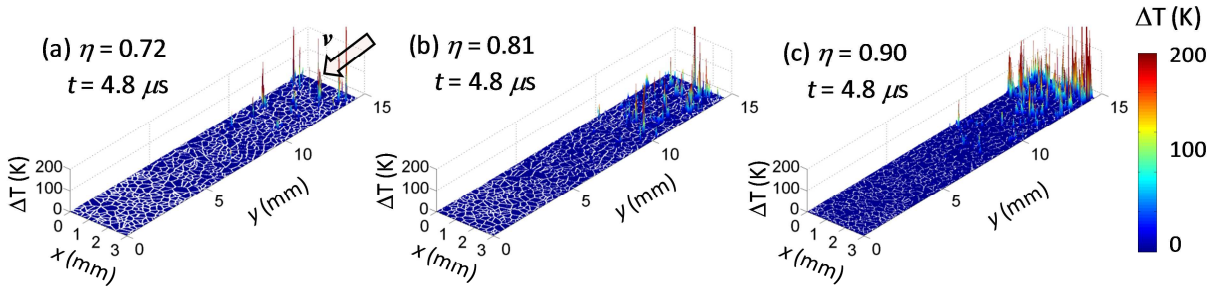

Fig. 4 Temperature fields in the grains (PBX in Figs. 3(a-c), $\eta = 0.72$ - 0.90, $v = 100$ ms^{-1}).

Effect of Grain Volume Fraction on Hotspot Distribution

In applications, it is desirable to have higher volume fraction for higher energy output. The effect of volume fraction is analyzed by deforming three PBX microstructures having initial volume fractions of $\eta = 0.72$, 0.81 and 0.90 [Figs. 3(a-c)], respectively. Figures 4(a-c) show the distribution of temperature at $t = 5.4$ μs. The impact velocity is $v = 100$ ms^{-1}. The calculations are performed using the loading configuration shown in Fig. 3(a). Clearly, the temperature increases with η for the same value of boundary displacement. For $\eta = 0.72$, the temperature increases are low and only occurs at locations of grain-grain interactions. Higher volume fractions lead to higher nominal stresses thereby enhancing grains-grain interactions and transgranular fracture. The overall effective wave speed also increases with the volume fraction. Consequently, under the same impact velocity microstructures having higher grain volume fractions experience high temperature increases over a larger domain.

The distributions of hotspots are distinct for each value of volume fraction. To analyze the effect of volume fraction, Figs. 5(a-c) show the RDFs and Figs. 5(d-f) shows the hotspot size distributions for the three calculations with initial volume fractions of $\eta = 0.72$, 0.81 and 0.90 at $t = 4.8$ μs. The impact velocity is $v = 100$ ms^{-1}. The maximum hotspot size shows no appreciable variation with the initial volume fraction. On the other hand, the average spacing between the hotspots (l_{avg}) is strongly influenced by the initial volume fraction. Specifically, l_{avg} decreases from 1.1 to 0.4 μm as the volume fraction is increased from $\eta = 0.72$ to 0.90. At lower packing densities, deformation of the binder reduces the stress level and prevents grain-grain interactions in the early part of loading, thereby reducing the formation of hotspots. This is in contrast to the behavior of GXs (Barua et al. [1]), where initial porosity does not significantly affect the hotspot spacing. The hotspot size distributions are similar for the different packing densities analyzed, indicating that the heating is primarily due to fracture and frictional dissipation occurring when the PBX is pressed to higher densities. It should be noted that this result is for impact velocities in the range between $v = 100$ and 200 ms^{-1}, and may not be applicable to scenarios with much higher impact velocities (e.g., during shock loading) where additional dissipation mechanisms (such as void collapse, jetting, etc) may influence the formation of hotspots.

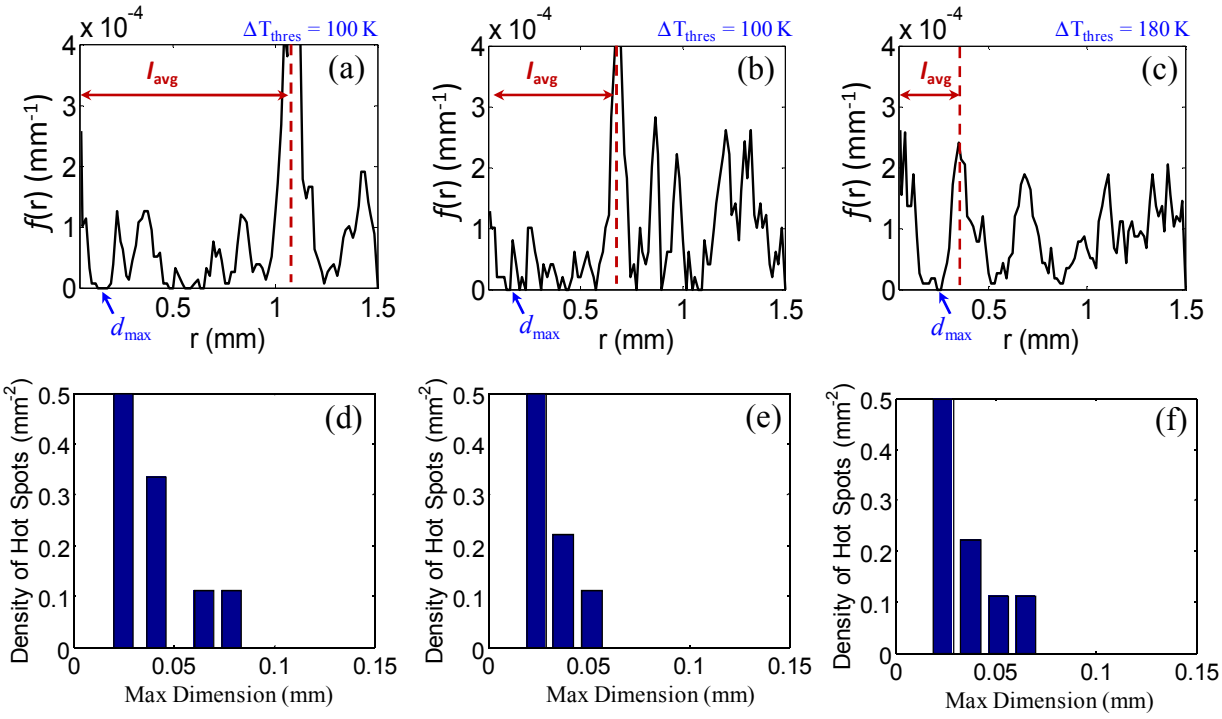

Fig. 5 RDFs of the temperature fields in microstructures of PBX having different grain volume fractions (a) η = 0.70, (b) η = 0.81, and (c) η = 0.90, and (d – f) the corresponding hotspot size distributions obtained using the maximum dimension method (v = 100 ms^{-1}, t = 4.8 μs).

Thermal Criticality of Hotspots

Hotspot distributions are analyzed using the scheme presented earlier to identify critical hotspots that may lead to ignition. The time (measured from the beginning of loading) at which a hotspot reaches the threshold condition [Eq. (1)] is taken as the time to criticality (t_c) and is obtained for different cases of impact velocity and grain volume fraction.

The effect of grain volume fraction is analyzed by comparing the criticality response of three PBX microstructures having initial volume fractions of η = 0.72, 0.81 and 0.90 [Figs. 3(a-c)]. Figure 6 shows the variation of the critical time t_c as a function of the boundary velocity, which is varied between v = 100 and 200 ms^{-1}. The calculations are performed using loading configuration shown in Fig. 3(a). The results are fitted to a curve of the form,

$$(v - v_c)^n t = C(\eta), \tag{2}$$

to illustrate the overall trends similar to what is done in Barua et al. [1]. Here, $C(\eta)$ is a function of initial porosity and v_c is the threshold velocity below which there is no ignition. The values of $C(\eta)$, n and v_c for the different microstructures analyzed are listed in Table 1. In general, as the boundary velocity increases, the time to criticality decreases. This is similar to the shock response of explosives [23-25].

Table 1. Parameters used in Eq. (2).

Microstructure	Grain volume fraction (η)	n	C	v_c (ms^{-1})
PBX–Monomodal	0.72	0.42	21.20	72.53
	0.81	0.41	19.18	63.11
	0.90	0.40	17.87	56.10

Overall, higher initial volume fraction η causes the PBX to be more sensitive (lower time to ignition). The variation in response with η is small at high impact velocities (v = 200 ms^{-1}), with a delay time of t_c ~2.5 μs for all values of η considered. The similarity in response is due to the fact that at high impact velocities, grain fracture (and fragmentation) occurs almost immediately upon impact, leading to high temperature increases in the grains near the impact surface. However, the sensitivity is significantly different at low impact velocities, with a critical time of $t_c = 4.1$ and 4.9 μs, for $\eta = 0.72$ and 0.90 respectively, at an impact velocity of $v = 100$ ms^{-1}.

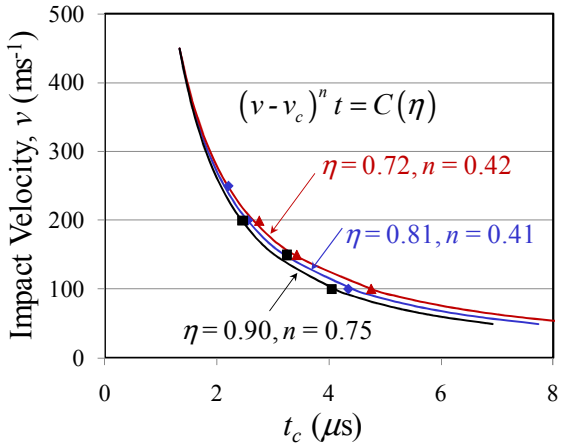

Fig. 6 Time to criticality for PBX having a range of initial grain volume fractions η = 0.72 – 0.90 (v = 100 – 200 ms^{-1}).

Conclusions

The analyses in this paper have focused on (1) the characterization of hotspot fields and (2) thermal criticality of hotspots resulting from the non-shock loading of polymer-bonded explosives (PBXs). For different HMX volume fractions, the study has yielded the critical impact velocity for ignition and critical time required for ignition as a function of material and impact velocity. The results show that fracture of energetic grains and subsequent friction along crack faces constitutes the most important heating mechanism in general. The grain volume fraction plays an important role in hotspot spacing with a lower grain volume fraction corresponding to a larger spacing between hotspots. The effect of the grain volume fraction on the time to criticality is most pronounced at low impact velocities and negligible at high impact velocities where localized fracture and friction near the impact face dominate.

Acknowledgement

The authors gratefully acknowledge support from the Air Force Research Laboratory (AFRL) at the Eglin AFB in Florida and the Defense Threat Reduction Agency (DTRA) (scientific officer: Dr. Suhithi Peiris). Calculations are carried out on parallel computers at the DPRL cluster at Georgia Tech.

References

[1] A. Barua, S. Kim, Y. Horie, and M. Zhou, "Ignition Criterion for Heterogeneous Energetic Materials Based on Hotspot Size-Temperature Threshold," *J. Appl. Phys.,* vol. 113, pp. 064906-064906-22, 2013.

[2] C. M. Tarver, S. K. Chidester, and A. L. Nichols, "Critical conditions for impact- and shock-induced hot spots in solid explosives," *J. Phys. Chem.,* 100 (1996) 5794-5799.

[3] M. R. Baer, "Modeling heterogeneous energetic materials at the mesoscale," *Thermochimica Acta,* 384 (2002) 351-367.

[4] J. E. Field, "Hot-spot ignition mechanisms for explosives," *Accounts Chem. Res.,* 25 (1992)489-496.

[5] R. Menikoff, "Pore collapse and hot spots in HMX," in *Shock Compression of Condensed Matter - 2003, Pts 1 and 2, Proceedings*. vol. 706, M. D. Furnish*, et al.*, Eds., ed Melville: Amer Inst Physics, (2004) 393-396.

[6] Y. Hamate and Y. Horie, "Ignition and detonation of solid explosives: a micromechanical burn model," *Shock Waves,* 16 (2006) 125-147.

[7] B. Asay, *Non-Shock Initiation of Explosives*. Berlin, Heidelberg :: Springer-Verlag Berlin Heidelberg, 2010.

[8] B. F. Henson, B. W. Asay, L. B. Smilowitz, and P. M. Dickson, "Ignition chemistry in HMX from thermal explosion to detonation," in *Shock Compression of Condensed Matter-2001, Pts 1 and 2, Proceedings*. vol. 620, M. D. Furnish*, et al.*, Eds., ed, (2002) 1069-1072.

[9] M. R. Baer, C. A. Hall, R. L. Gustavsen, D. E. Hooks, and S. A. Sheffield, "Isentropic loading experiments of a plastic bonded explosive and constituents," *J. Appl. Phys.,* 101 (2007) p. 12.

[10] W. M. Trott, M. R. Baer, J. N. Castaneda, L. C. Chhabildas, and J. R. Asay, "Investigation of the mesoscopic scale response of low-density pressings of granular sugar under impact," *J. Appl. Phys.,* vol. 101, 2007.

[11] R. A. Austin, D. L. McDowell, and D. J. Benson, "Numerical simulation of shock wave propagation in spatially-resolved particle systems," *Model. Simul. Mater. Sci. Eng.,* 14 (2006) 537-561.

[12] D. J. Benson and P. Conley, "Eulerian finite-element simulations of experimentally acquired HMX microstructures," *Model. Simul. Mater. Sci. Eng.,* 7 (1999) 333-354.

[13] D. B. Hayes and D. E. Mitchell, *Constitutive equation for the shock response of porous hexanitrostilbene (HNS) explosive*, 1978.

[14] R. Menikoff, "Compaction wave profiles in granular HMX," Los Alamos National Laboratory, Los Alamos, NM 87544.

[15] R. Menikoff, "Granular explosives and initiation sensitivity," *Detonation Theory & Application, T14,* vol. Special Feature, 2000.

[16] H. Kim, A. Lagutchev, and D. D. Dlott, "Surface and interface spectroscopy of high explosives and binders: HMX and Estane," *Propellants Explos. Pyrotech.,*31 (2006) 116-123.

[17] A. Tokmakoff, M. D. Fayer, and D. D. Dlott, "Chemical-Reaction Inititation and Hot-Spot Formation in Shocked Energetic Molecular Materials," *J. Phys. Chem.,* 97 (1993) 1901-1913.

[18] R. Panchadhara and K. A. Gonthier, "Mesoscale analysis of volumetric and surface dissipation in granular explosive induced by uniaxial deformation waves," *Shock Waves,* 21 (2011) 43-61.

[19] A. Barua and M. Zhou, "A Lagrangian Framework for Analyzing Microstructural Level Response of Polymer-Bonded Explosives," *Model. Simul. Mater. Sci. Eng.,* 19 (2011) p. 24.

[20] A. Barua, Y. Horie, and M. Zhou, "Energy localization in HMX-Estane polymer-bonded explosives during impact loading," *J. Appl. Phys.,* 111 (2012) p. 11.

[21] A. Barua and M. Zhou, "Computational analysis of temperature rises in microstructures of HMX-Estane PBXs," *Comput. Mech.,* (2012) 1-9.

[22] J. K. Dienes, Q. H. Zuo, and J. D. Kershner, "Impact initiation of explosives and propellants via statistical crack mechanics (vol 54, pg 1237, 2006)," *J. Mech. Phys. Solids,* 54 (2006) 2235-2240.

[23] H. R. James, "An extension to the critical energy criterion used to predict shock initiation thresholds," *Propellants Explos. Pyrotech.,* 21, (1996) 8-13.

[24] H. R. James, "Shock initiation thresholds for insensitive high explosives," in *Shock Compression of Condensed Matter - 2007, Pts 1 and 2*. vol. 955, M. Elert*, et al.*, Eds., ed Melville: Amer Inst Physics, (2007) 937-940.

[25] H. R. James, R. J. Haskins, and M. D. Cook, "Prompt shock initiation of cased explosives by projectile impact," *Propellants Explos. Pyrotech.,* 21 (1996) 251-257.

Explosion, Shock Wave and High-Energy Reaction Phenomena II
10.4028/www.scientific.net/MSF.767

Computational Analysis of Ignition in Heterogeneous Energetic Materials
10.4028/www.scientific.net/MSF.767.13